A modeling approach for electrokinetic transport in double-porosity media

López-Vizcaíno, Rubén; Cabrera, Virginia; Sprocati, Riccardo; Muniruzzaman, Muhammad; Rolle, Massimo; Navarro, Vicente; Yustres, Ángel

Published in:
Electrochimica Acta

Link to article, DOI:
10.1016/j.electacta.2022.141139

Publication date:
2022

Document Version
Publisher's PDF, also known as Version of record

Electrochimica Acta 431 (2022) 141139

Contents lists available at ScienceDirect

Electrochimica Acta

journal homepage: www.journals.elsevier.com/electrochimica-acta

A modeling approach for electrokinetic transport in double-porosity media

Rubén López-Vizcaíno [a,*], Virginia Cabrera [a], Riccardo Sprocati [b], Muhammad Muniruzzaman [c], Massimo Rolle [b,d], Vicente Navarro [a], Ángel Yustres [a,*]

[a] Geoenvironmental Group, Department of Civil Engineering and Construction, Civil Engineering School, University of Castilla-La Mancha, Avda. Camilo José Cela s/n, 13071 Ciudad Real, Spain
[b] Department of Environmental and Resource Engineering, Technical University of Denmark, Bygningstorvet, Building 115, 2800 Kongens Lyngby, Denmark
[c] Geological Survey of Finland, Vuorimiehentie 5, PO Box 96, 02151 Espoo, Finland
[d] Institute for Applied Geosciences, Technical University of Darmstadt, Schnittspahnstr. 9, 64287 Darmstadt, Germany

ARTICLE INFO

KEYWORDS:
Donnan potential
Double porosity
Electrokinetic remediation
Electromigration
Active clay
Diffuse layer

ABSTRACT

Electrokinetic techniques have attracted considerable attention due to their competitive advantage in enhancing transport phenomena and remediation of low permeability soils. However, many types of low-permeability porous media, such as active clays like bentonite, present a double porosity structure that strongly affects mass transfer processes. In this work, we develop a modeling approach to simulate electrokinetic transport in double porosity media. The proposed model is based on the previously released code M4EKR and explicitly considers the transport due to electromigration as well the effects of the electrical diffuse layer in charged porous media. For this purpose, two modeling levels have been established: one associated with the soil macrostructure (bulk water) and the other with the microstructure (diffuse layer). At the latter level, the effect of the electrostatic interactions imposed by the negative charge of the clay particles is modeled with a Donnan approach. The comparison of the results between synthetic cases in single and double porosity systems shows the fundamental role of the microstructural modeling level. High enrichment of cations and, therefore, high cationic fluxes are produced in such microstructural level. These mechanisms significantly modify the extent of cation transport by electromigration and, thus, directly influence the transport of other species determined by the electrostatic interactions.

1. Introduction

Electrokinetic (EK) soil remediation has been proposed as a treatment technology due to its potential effectiveness for in-situ contaminant removal in low permeability porous media. In addition, EK techniques have also been used in other fields of science and engineering with the aim of enhancing the transport of species and/or fluids through low permeability porous matrices where other conventional technologies showed limitations [1–8]. EK techniques are based on the application of an electric potential gradient by means of electrode pairs (anodes/cathodes) placed in the porous media. The electric potential gradient acts as a driving force for different electrokinetic transport mechanisms that take place simultaneously such as electroosmosis, electromigration and electrophoresis [9]. Additionally, other transport processes such as diffusion and advection can occur, driven by chemical concentration gradients and hydraulic gradients, respectively.

The occurrence of this multitude of transport processes makes it necessary to develop numerical models capable of simulating complex interactions. A particular advantage of process-based numerical models is that they allow the description of complex systems, the analysis of each individual phenomena and their coupled interactions. In the last decades, considerable research effort has been dedicated to quantitatively describe different physicochemical processes, and the research community has developed a wide variety of mathematical models [10–13]. The most advanced solute transport codes are based on the solution of the Nernst-Plank-Poisson equations, which account for the transport of charged species in porous media considering the effect of Coulombic interactions in natural transport [14–16] and under the application of an external electric field [12,17–20]. Although there are codes that can account for Coulombic interactions and surface charge effects [13,21–25], the models describing electrokinetic transport are typically designed for single-porosity domains.

* Corresponding authors: Geoenvironmental Group, Department of Civil Engineering and Construction, Civil Engineering School, University of Castilla-La Mancha, Avda. Camilo José Cela s/n, 13071 Ciudad Real, Spain.
E-mail addresses: ruben.lopezvizcaino@uclm.es (R. López-Vizcaíno), angel.yustres@uclm.es (Á. Yustres).

https://doi.org/10.1016/j.electacta.2022.141139
Received 21 June 2022; Received in revised form 30 August 2022; Accepted 1 September 2022
Available online 4 September 2022

However, soils with very low hydraulic conductivity often contain large fractions of active clays such as bentonites and have been described using two modeling levels [26–32]. The microstructural modeling level allows the description of the processes taking place in intra-aggregate pores (Fig. 1a) which corresponds to the void volume affected by charged surfaces (equivalent to the diffuse layer volume [33]), whereas the macrostructural modeling level accounts for the processes occurring in the pores between the clay aggregates (inter-aggregate voids in Fig. 1a) [34], which corresponds to the free water volume [33]. Although reactive transport models, incorporating dual-continuum formulation for clay media, exist for simulating transport in low-permeability media [14,23,24,35–37], they have mainly been developed for the study of natural transport systems and the adoption of such approaches for EK systems has been rarely attempted [21].

In this study, we present an approach to simulate electrokinetic transport by electromigration in double-porosity porous media. The approach is implemented as a new, extended version of the previously published code, M4EKR, [40,41] (multiphysics model for the simulation of reactive transport processes in porous media under the action of an electric field). The approach is based on Donnan equilibrium to determine the species distribution between the macrostructural and microstructural levels (i.e., free water and diffuse layer) [14,35]. The model has been used to investigate the transport of ionic species in an active clay with two modeling levels, analyzing the influence of the microstructure on the mobilization of the chemical species. To this end, the model was first tested under natural diffusive transport conditions. The outcomes of the proposed approach were compared with an analytical solution and with the results of the software PHREEQC. Subsequently, electrokinetic transport was considered and the results of the developed M4EKR approach were verified in a single-porosity with the data of a recent numerical study [17]. Finally, we used the developed approach to simulate EK transport in a double-porosity system (MX-80 bentonite-like) and to evaluate the influence of the microstructural domain on the transport of a charged species by electromigration. We analyzed different scenarios considering different values of the ionic strength of the porewater.

2. Mathematical formulation

A double porosity approach has been adopted to define the structure of charged porous media, such as clay. This conceptual model considers the internal composition of clays through a macroscopic model in which two interconnected continua maintain a mass-exchange equilibrium [42]: (i) the microstructural modeling level, which simulates the effect of the processes occurring at the intra-aggregate pores affected by the electric fields imposed by the negatively charged surface of the clay sheets, and (ii) the macrostructural modeling level for the rest of the porespace [43]. We consider that the diffusive layer (DL) is linked to microstructural modeling level, where a high concentration of counterions neutralize the excess of charge from clay surface. The rest of the porewater volume is called free water, where the solution is electrically neutral, and corresponds with the macrostructural modeling level as illustrated in Fig. 1c [14,35,44].

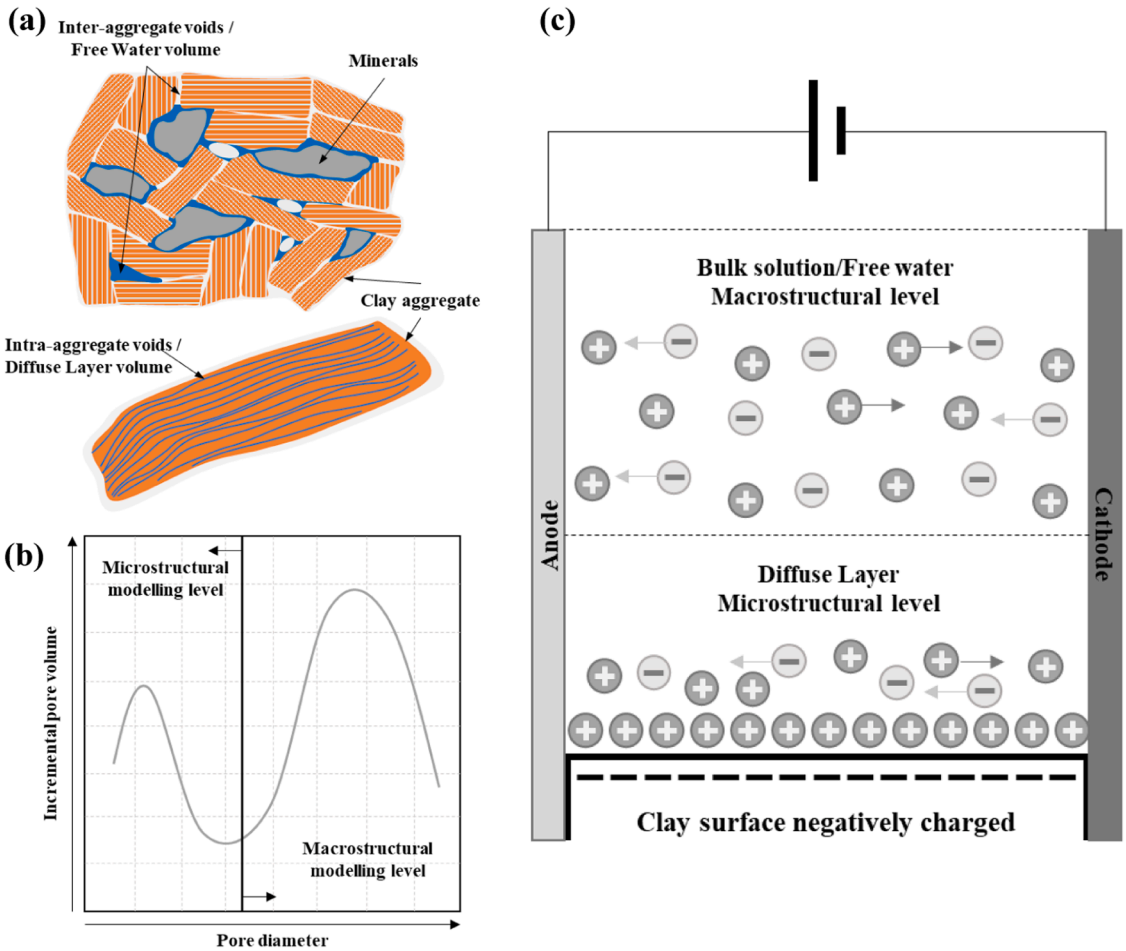

Fig. 1. (a) Schematic of double-porosity media (adapted from [38]). (b) Qualitative distribution of incremental pore volume for a double-porosity medium from a mercury intrusion porosimeter test (adapted from [39]). (c) Conceptual model of a double-porosity-EK system.

2.1. Donnan equilibrium approach

The Donnan equilibrium approach [35,45] assumes that the electrochemical potential of the *i* th species at the generic modeling level *L*, μ_i^L, must be equal both in macro (*M*) and microstructural (*m*) levels ($\mu_i^M = \mu_i^m$). Considering the definition of μ_i^L, the electrochemical potential at any structural level is given by:

$$\mu_i^L = \mu_{0i} + RT\ln a_i^L + z_i F\psi^L \tag{1}$$

where μ_{0i}, a_i^L and z_i are the electrochemical potential in standard conditions, the chemical activity and the charge of the i th species, respectively, *R* is the ideal gas constant, *F* is the Faraday constant, and ψ^L is the electric potential at the corresponding modeling level which is the sum of several contributions. In the M4EKR model, $\psi^L$is calculated according to the following expression:

$$\psi^L = \psi_{ce}^L + \psi_{ext}^L \tag{2}$$

where ψ_{ce}^L is the electrical potential that includes the electrostatic effects generated by multicomponent diffusion and charged surface properties of the clay [14,46,47], and ψ_{ext}^L is the electric potential applied externally.

The chemical activity can be defined as a "effective concentration" of i th species into the real mixtures. In liquid solutions it is calculated as $a_i^L = \gamma_i^L c_i^L$ where γ_i^L is the activity coefficient (that represents the deviations from ideal behavior) and $c_i^L$the molality. Considering the above, and assuming that the activity coefficients are equal in the micro and macrostructural levels ($\gamma_i^m = \gamma_i^M$), the Donnan equilibrium which regulates the distribution of the species in both modeling levels can be defined as [48]:

$$c_i^m = c_i^M \exp\left(\frac{-z_i F\psi_D}{RT}\right) \tag{3}$$

where the concentrations of the i th species in the micro and macrostructural levels are c_i^m and c_i^M, respectively.

The Donnan potential, ψ_D is defined as:

$$\psi_D = \psi^M - \psi^m \tag{4}$$

The procedure for the calculation of the Donnan potential, taking into account the geochemical system selected in this work is described in detail in the Supplementary Material.

2.2. Transport of chemical species

The spatial and temporal distribution of each i th species can be obtained by solving the general mass balance equation:

$$\frac{\partial m_i}{\partial t} + \nabla\cdot\mathbf{j}_{tot,i} - f_i = 0 \tag{5}$$

where m_i is the total mass per unit of volume, $\mathbf{j}_{tot,i}$is the total flux and f_i is the sink/source term of the i th species, respectively. The total mass of the i th species is calculated by the sum of the individual mass in the macrostructural, m_i^M, and microstructural levels, m_i^m, which are defined as:

$$m_i = m_i^M + m_i^m = c_i^M Sr^M \phi^M + c_i^m Sr^m \phi^m \tag{6}$$

where Sr^L is the degree of saturation and $\phi^L$is the porosity associated with the modeling level L. The total flux $\mathbf{j}_{tot,i}$, similarly to the mass, is constituted by the contribution of the fluxes generated at each modeling level ($\mathbf{j}_{tot,i} = \sum^L \mathbf{j}_{tot,i}^L$), which is defined by the Nernst-Planck equation [22,[44,45,49,50]. As a result, $\mathbf{j}_{tot,i}^L$ can be obtained by the sum of several terms related to the different transport mechanisms involved in the expression:

$$\mathbf{j}_{tot,i}^L = \mathbf{j}_{dif,i}^L + \mathbf{j}_{ce,i}^L + \mathbf{j}_{em,i}^L + \mathbf{j}_{adv,i}^L \tag{7}$$

where $\mathbf{j}_{dif,i}^L$ is the diffusive flux, $\mathbf{j}_{ce,i}^L$ is the flux generated by Coulombic effects derived from the local charge-neutrality constraint during multicomponent transport and charged clay surfaces [14,46], $\mathbf{j}_{em,i}^L$ is the electromigration flux generated by the application of an external electric potential gradient, and $\mathbf{j}_{adv,i}^L$ is the contribution of advective fluxes (driven by hydraulic and electroosmotic gradients). These terms are calculated according to the following expressions:

$$\mathbf{j}_{dif,i}^L = -D_{e,i}^L c_i^L \nabla\left(\ln a_i^L\right) \tag{8}$$

$$\mathbf{j}_{ce,i}^L = -u_{e,i}^L c_i^L \nabla\psi_{ce}^L \tag{9}$$

$$\mathbf{j}_{em,i}^L = -u_{e,i}^L c_i^L \nabla\psi_{ext}^L \tag{10}$$

$$\mathbf{j}_{adv,i}^L = c_i^L\left(\mathbf{q}_h^L + \mathbf{q}_{eo}^L\right) \tag{11}$$

The terms $\mathbf{q}_h^L$ and $\mathbf{q}_{eo}^L$ are the water fluxes representing the hydraulic and electroosmotic fluxes, respectively, $u_{e,i}^L$ is the effective ionic mobility [51,52] and $D_{e,i}^L$ is the effective diffusion coefficient [40] calculated as:

$$u_{e,i}^L = \frac{z_i F D_{e,i}^L}{RT} \tag{12}$$

$$D_{e,i}^L = \phi^L Sr^L \tau^L D_{o,i} \tag{13}$$

where $D_{o,i}$ is the aqueous diffusion coefficient of the i th species in water. Sr^L and τ^L are the tortuosity and the degree of saturation of the L-th modeling level, respectively.

2.3. Transport of electric current

Poisson's equation can be obtained from both Gauss's law and the conservation of charge, provided that the electrical properties of the medium are constant [53,54]. The proposed M4EKR model implements a formulation based on the conservation of charge and the electroneutrality condition at both structural levels [38]. Such approach is equivalent to the use of Gauss's law, as proposed by other authors [12,17,19], but with certain practical advantages from a numerical and conceptual point of view, as discussed in detail in [55].

The electroneutrality condition in the macro and microstructural levels is defined with the following expressions:

$$\sum_{i=1}^{N} z_i c_i^M = 0 \tag{14}$$

$$\sum_{i=1}^{N} z_i c_i^m + Q_{clay} = 0 \tag{15}$$

where Q_{clay} is the charge concentration of clay particles defined as:

$$Q_{clay} = (1-\phi)\frac{\rho_s}{\phi^m} CEC \tag{16}$$

where *CEC* is the cation exchange capacity, ρ_s is the density of the solid particles and ϕ is the total porosity ($\phi = \phi^M + \phi^m$).

Starting from an electrically balanced initial condition with no charge accumulation and taking into account that during an EK application no phenomenon generates charge accumulation [56], the electrical charge balance can be expressed as:

$$\nabla\cdot\mathbf{i} = 0 \tag{17}$$

The current density $\mathbf{i}$ can be defined by the sum of the contributions

from the transport of ionic species in the liquid phase ($\mathbf{i}^{L}$) and the conduction in the solid matrix (Ohm's Law)[57]:

$$\mathbf{i} = \sigma_s \nabla \psi_{ext} + \sum^{L} \mathbf{i}^{L} \tag{18}$$

where σ_s is the apparent electrical conductivity of the soil and $\mathbf{i}^{L}$is expressed as:

$$\mathbf{i}^{L} = F \sum_{i=1}^{N} z_i \mathbf{j}^{L}_{tot,i} \tag{19}$$

In contrast, considering that the current density is higher than zero when an external electric field is applied, either by conduction in the solid matrix or by the charge carried by the ionic species in the porewater mostly by electromigration [17,54,57], it can be assumed that $\mathbf{i} = 0$ in the absence of an external electric potential ($\psi^{L}_{ext} = 0;\ \mathbf{j}^{L}_{em,i} = 0$). In this case, Eq. (19) can be rewritten as:

$$\mathbf{i}^{L} = F \sum_{i=1}^{N} z_i \left(\mathbf{j}^{L}_{dif,i} + \mathbf{j}^{L}_{ce,i} \right) = F \sum_{i=1}^{N} z_i \left(- D^{L}_{e,i} c^{L}_i \nabla \left(\ln a^{L}_i \right) - u^{L}_{e,i} c^{L}_i \nabla \left(\psi^{L}_{ce} \right) \right) = 0 \tag{20}$$

The gradient of the electric potential can then be calculated by rearranging Eq. (20) [14,46]:

$$\nabla \psi^{L}_{ce} = - \frac{\sum_{i=1}^{N} z_i D^{L}_{e,i} c^{L}_i \nabla \left(\ln a^{L}_i \right)}{\sum_{i=1}^{N} z_i u^{L}_{e,i} c^{L}_i} \tag{21}$$

2.4. Numerical model implementation

The proposed version of the M4EKR model has been fully implemented in COMSOL Multiphysics. This platform is a differential equation solver based on the application of the finite element method with Lagrange multipliers. In this work, all equations have been implemented using the constitutive models presented above, without pre-programmed COMSOL modules. In the scenarios investigated, we consider four dissolved charged species (although without loss of generality, it can be expanded to the desired number of species) and, consequently, a total of 5 partial differential equations: four of them to solve the mass balance of the corresponding species and one to solve the electric charge balance. The state variables are the concentration in the macrostructural level of each ion (c^{M}_i) and the external electric potential (ψ^{L}_{ext}). The Donnan potential is calculated as a quadratic equation using the formula described in Supplementary Material (Section 3).

The code solves all the balance equations simultaneously, using a monolithic, fully coupled approach. COMSOL manages pre-processing (discretization, initial and boundary conditions), the solution of the system of partial differential equations (PDE), and the post-processing of the results (Fig. 2).

3. Description of the simulation exercises

To analyze the capabilities of the proposed M4EKR model, a series of simulations have been performed to: (i) verify diffusive transport in double porosity media, (ii) test electrokinetic transport in single porosity media, and (iii) explore electrokinetic transport in double porosity media. For this purpose, simulation exercises (SE) have been carried out using different configurations (Fig. 3) and considering four ideal species: A^{+}, B^{-}, C^{+}, D^{-}. In all simulations the contribution of hydraulic and electroosmotic fluxes ($\mathbf{j}^{L}_{adv,i}$) has been disregarded as a first approximation to the problem. Consequently, it is assumed that the main transport phenomena of charged species are diffusion and electromigration.

Fig. 3a illustrates the first setup representing a one-dimensional domain with a porous medium similar to the Opalinus clay described in a previous study [14]. The porous medium is in contact at the left boundary with a salt solution contained in a large reservoir so that it can be assumed at a constant concentration. The right boundary condition is a no-flux condition.

Fig. 3b presents a similar configuration but formed by two domains with different initial porewater concentrations. In this setup, the imposed boundary conditions are no-flux on both sides. Considering these aspects, the diffusive transport is verified in the following three stages. First, a simulation exercise (SE 1) has been performed to verify the diffusion through the micro- and macrostructural levels independently, by setting the porosity of the other level equal to zero to compare the results obtained directly with the analytical solution of one dimensional diffusive transport in a semi-infinite domain [58]. Subsequently, a second simulation exercise (SE 2) has been performed to test the transport through both structural levels at the same time. For this purpose, a test including surface/solution interactions has been simulated using the same configuration (Fig. 3a) and the results have been compared with those obtained with the code PHREEQC. In the third simulation exercise, the diffusive flux through a double-porosity medium with two domains of different initial concentration has been examined (Fig. 3b). For this purpose, a benchmark proposed by Tournassat and Steefel [36] has been simulated (SE3) and the results have been compared with those obtained by the software CrunchClay and 3-Diff [36]. The parameters used in simulation exercises considering natural transport are shown in Table 1.

The initial chemical composition of the porewater domain and the concentration of the source reservoir is presented in Table 2.

Electrokinetic transport was investigated in SE 4 and SE 5 as shown in Figs. 3c and 3d, respectively. SE 4 considers EK transport in a single porosity medium, whereas SE 5 illustrates the capabilities of the proposed M4EKR model to evaluate electrokinetic transport in double porosity media. The MX-80 bentonite, which has been extensively studied [59–61], was selected as representative double-porosity material. The simulated setups (Fig. 3c and 3d) are based on a one-dimensional system, consisting of a 1 m long compartment for the porous media and two large volume reservoirs. In this way, it is possible to neglect the effects of electrolysis reactions and to assume a constant concentration in the electrode reservoirs.

The three scenarios analyzed consider that the ionic strength (IS) of

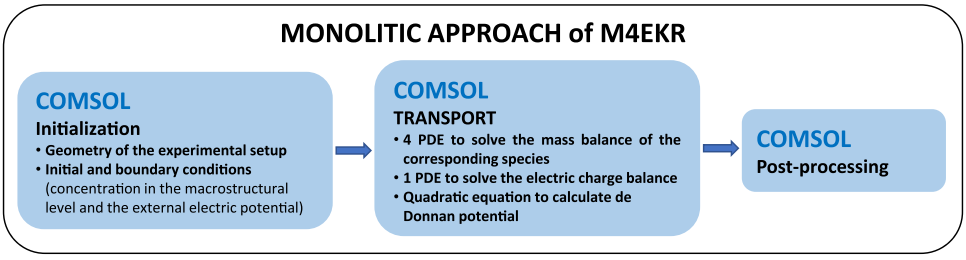

Fig. 2. Schematic illustration of the M4EKR numerical code to simulate electrokinetic transport in double-porosity media.

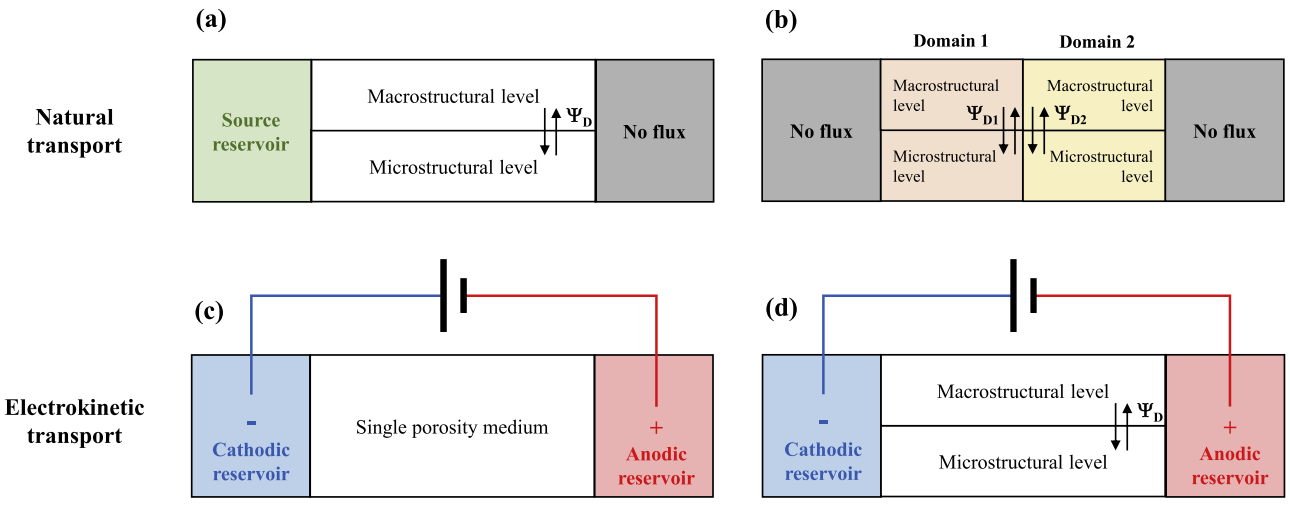

Fig. 3. Scheme of the different configurations selected for conducting the simulation exercises (SE): (a) diffusive transport in a double porosity medium (SE 1 and SE 2), (b) diffusive transport between two different double porosity media- (SE 3), (c) electrokinetic transport in a single porosity medium (SE 4), and (d) electrokinetic transport in a double porosity medium (SE 5).

Table 1
Parameters used in the natural transport simulations (simulation exercises SE 1, SE 2 and SE 3).

			SE 1 Diffusion in individual levels (Fig. 3a)		SE 2 Diffusion and solid/solution interactions (Fig. 3a)	SE 3 Diffusion in a double-porosity medium with two initial concentration domains (Fig. 3b)	
Parameter	Description	Unit	Transport only in Macro	Transport only in micro	Transport both in micro and Macro	Domain 1	Domain 2
ϕ^M	Porosity at Macro	–	0.08	0.00	0.08	0.3	0.3
ϕ^m	Porosity at micro	–	0.00	0.08	0.08	0.3	0.3
τ^M	Tortuosity at Macro	–	0.16	0.00	0.16	1	1
τ^m	Tortuosity at micro	–	0.00	0.16	0.16	1	1
t	Time	s	1.0×10^8			1.0×10^3	
L	Domain length	m	1			3.0×10^{-3}	
T	T emperature	°C	25			25	
CEC	Cation exchange capacity	$mol\,kg^{-1}$	0.1128			0.1000	0.1000
σ_s	Apparent electrical conductivity	$S\,m^{-1}$	0			0	
ρ_d	Dry density	$kg\,m^{-3}$	2270			1000	
$D_{o,i}$	Aqueous diffusion coefficient	$m^2 s^{-1}$	1.0×10^{-9}*			A^+	1.3×10^{-9}**
						B^-	2.1×10^{-9}**
						C^+	1.3×10^{-9}**
						D^-	2.1×10^{-9}**

* Same value for the species A^+, B^-, $C^+$and D^-.
** Same value for the two domains.

Table 2
Initial chemical composition of the porewater and source reservoir composition for a system of ideal ions (units $mol\,kg^{-1}_{water}$) to conduct the SE 1, SE 2 and SE 3.

			A^+	B^-	C^+	D^-
SE 1	Transport only in Macro	Source, c_i^M	1.0×10^{-4}	1.0×10^{-4}	2.5×10^{-3}	2.5×10^{-3}
		Porewater, c_i^M	1.0×10^{-3}	1.0×10^{-3}	1.0×10^{-3}	1.0×10^{-3}
	Transport only in micro	Source, c_i^m	1.2×10^{-1}	8.1×10^{-8}	3.1×10^{0}	2.0×10^{-6}
		Porewater, c_i^m	1.6×10^{0}	6.2×10^{-7}	1.6×10^{0}	6.2×10^{-7}
SE 2*	Transport both in micro and Macro	Source, c_i^M	–	–	1.0×10^{-3}	1.0×10^{-3}
		Porewater, c_i^M	1.0×10^{-3}	1.0×10^{-3}	–	–
		Source, c_i^m	–	–	3.2×10^{0}	3.1×10^{-7}
		Porewater, c_i^m	3.2×10^{0}	3.1×10^{-7}	–	–
SE 3**	Domain 1	Porewater, c_i^M	1.0×10^{-2}	1.0×10^{-2}	1.0×10^{-12}	1.0×10^{-12}
		Porewater, c_i^m	3.3×10^{-1}	3.0×10^{-4}	3.3×10^{-11}	3.0×10^{-14}
	Domain 2	Porewater, c_i^M	1.0×10^{-1}	1.0×10^{-1}	1.0×10^{-30}	1.0×10^{-30}
		Porewater, c_i^m	3.6×10^{-1}	2.8×10^{-2}	3.6×10^{-30}	2.8×10^{-31}

* The results of SE 2 are compared with PHREEQC where pH is fixed to 7.0.
** The results of SE 3 are compared with CrunchClay where pH is fixed to 7.0.

the porewater at the beginning of the tests is lower (IS_{Low}), equal (IS_{Equal}) or higher (IS_{High}) than the one of the cathodic electrolyte. This allowed us to evaluate the influence of the ionic strength of the porewater and of the catholyte on the transport of the different species included in the system [62]. Note that the total porosity in both EK simulations is equal to 0.4. In SE 5, the distribution-ratio between the macro and microstructural porosities selected was 50% for each modeling level (realistic value according to the literature [44,59]). The parameters used in the electrokinetic transport simulations are shown in Table 3.

The initial location of the ionic species, both in the porous media and in the electrode reservoirs is the same regardless of the three scenarios evaluated. Initially, the species A^+ and B^- are only found in the catholyte, whereas C^+ and D^- in the anolyte and porewater. The initial concentration of porewater and anolyte used in each of the evaluated scenarios is shown in Table 4, considering that the concentrations used in the simulations with the single-porosity model (SE 4) are those of the macrostructural level in the double-porosity approach (SE 5). The initial concentration of the species A^+ and B^- in the catholyte is, constant (10^{-2} mol kg^{-1}_{water}) in all three scenarios. In all simulations, Dirichlet-type boundary conditions have been applied following the concentration values of the catholyte and anolyte in each case.

In the simulation exercise exploring EK transport in double-porosity media (SE 5), we considered two different scenarios with restricted and free microstructural transport, respectively. These assumptions are implemented in the proposed M4EKR model by modifying the tortuosity value of microstructural modeling level, 0.0 for restricted transport simulation and 0.4 for free microstructural transport.

4. Results and discussion

4.1. Diffusive transport in double porosity media

The simulation of diffusive transport has been tested at each structural level independently versus the analytical solution (SE 1) and the results obtained for the micro and macrostructural levels are presented in Figures SM1 and SM2 in the Supplementary Material document and show the capability of the model to correctly describe diffusive transport in both levels.

The results of the test considering surface/solution interactions with two structural levels (SE 2) are shown in Fig. 4.

There is a very good match between the results of the M4EKR model and PHREEQC. The profiles show the replacement of the cations (A^+ for C^+) due to their interactions with the surface in the microstructural level and also the affection to the concentrations at the macrostructural level. The distribution of the anions (B^- for D^-) in both levels is directly affected by the cations due to the electroneutrality condition. It can be observed how the surface electrical effects of the simulated porous medium (Opalinus clay) influence the ion concentration at the microstructural level, where the cation concentrations are orders of magnitude higher, and the anions concentrations are orders of magnitude lower than at the macrostructural level.

The outcomes of the last natural transport case SE 3, considering diffusion and charge interactions in two adjacent double-porosity domains, can be found in Figures SM3, SM4 and SM5 in the Supplementary Material. The computed spatial distribution of the species concentrations in the macro and microstructural levels, and the evolution of the Donnan potential are shown at two different times. The results illustrate the capability of the M4EKR model to simulate transport and Coulombic interactions in spatially distributed double-domain porous media with different initial conditions and the very good agreement with other simulators [36].

Table 3
Parameters used in the EK transport simulations (simulation exercises SE 4 and SE 5).

Parameter	Description	Unit	SE 4	SE 5
ϕ^M	Porosity at Macro	–	0.4	0.2
ϕ^m	Porosity at micro	–	0	0.2
τ^M	Tortuosity at Macro	–	0.4	0.4
τ^m	Tortuosity at micro	–	0	0.4
CEC	Cation exchange capacity	mol kg^{-1}	0	−0.88
t	Time	day	6	
T	T emperature	°C	25	
$\nabla\psi_{ext}$	External electrical potential gradient	V cm^{-1}	1	
σ_s	Apparent electrical conductivity	S m^{-1}	0	
ρ_s	Density of solid particles	kg m^{-3}	2750	
$D_{o,i}$*	Aqueous diffusion coefficient	$m^2 s^{-1}$	1.0×10^{-9}	

* Same value for the species A^+, B^-, $C^+$and D^-.

Table 4
Initial chemical composition of the porewater and anolyte composition for a system of ideal ions (units mol kg^{-1}_{water}) to conduct the SE 4 and SE 5. Adapted from Sprocati and Rolle [17].

		A^+	B^-	C^+	D^-	ψ_D* (V)
IS_{Low}	Anolyte	0	0	2.5×10^{-3}	2.5×10^{-3}	–
	Porewater, c_i^M	0	0	2.5×10^{-3}	2.5×10^{-3}	−0.205
	Porewater, c_i^m*	0	0	7.257	8.6×10^{-7}	
IS_{Equal}	Anolyte	0	0	1.0×10^{-2}	1.0×10^{-2}	–
	Porewater, c_i^M	0	0	1.0×10^{-2}	1.0×10^{-2}	−0.169
	Porewater, c_i^m*	0	0	7.259	1.4×10^{-5}	
IS_{High}	Anolyte	0	0	4.0×10^{-2}	4.0×10^{-2}	–
	Porewater, c_i^M	0	0	4.0×10^{-2}	4.0×10^{-2}	−0.134
	Porewater, c_i^m*	0	0	7.26	2.2×10^{-4}	

* Only for SE 5.

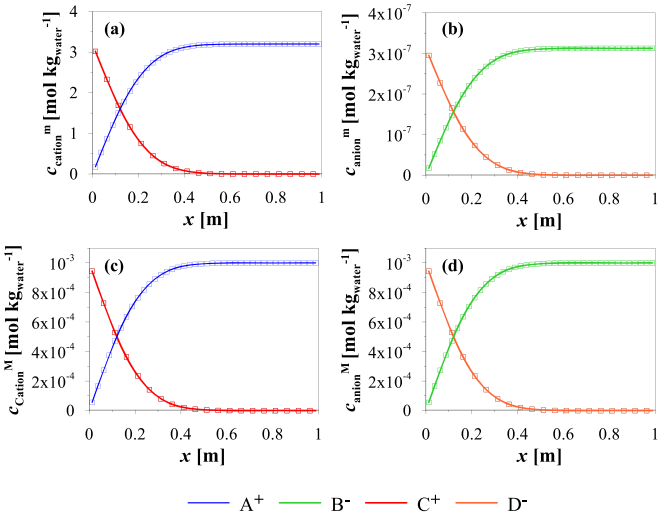

Fig. 4. Simulation exercise 2. Concentration distribution, at $t = 10^8$ s, of: cations A^+ and C^+ in the (a) micro and (c) macrostructure; anions B^- and D^- in the (b) micro and (d) macrostructure. Markers indicate results from PHREEQC whereas lines are the results of M4EKR model.

4.2. Electrokinetic transport in single-porosity media

This simulation exercise (SE 4) involves the three cases with different ionic strength, described Section 3. These electrokinetic transport problems were simulated by adapting the double-porosity M4EKR model to domains with a single structural level by cancelling the microstructural porosity and tortuosity, the Donnan potential and by setting *CEC*=0 mol kg^{-1}. We analyzed the same variables reported in the work of Sprocati and Rolle [17] to test the proposed M4EKR implementation. The results are illustrated in Fig. 5.

The results obtained with the M4EKR model fit those used as a

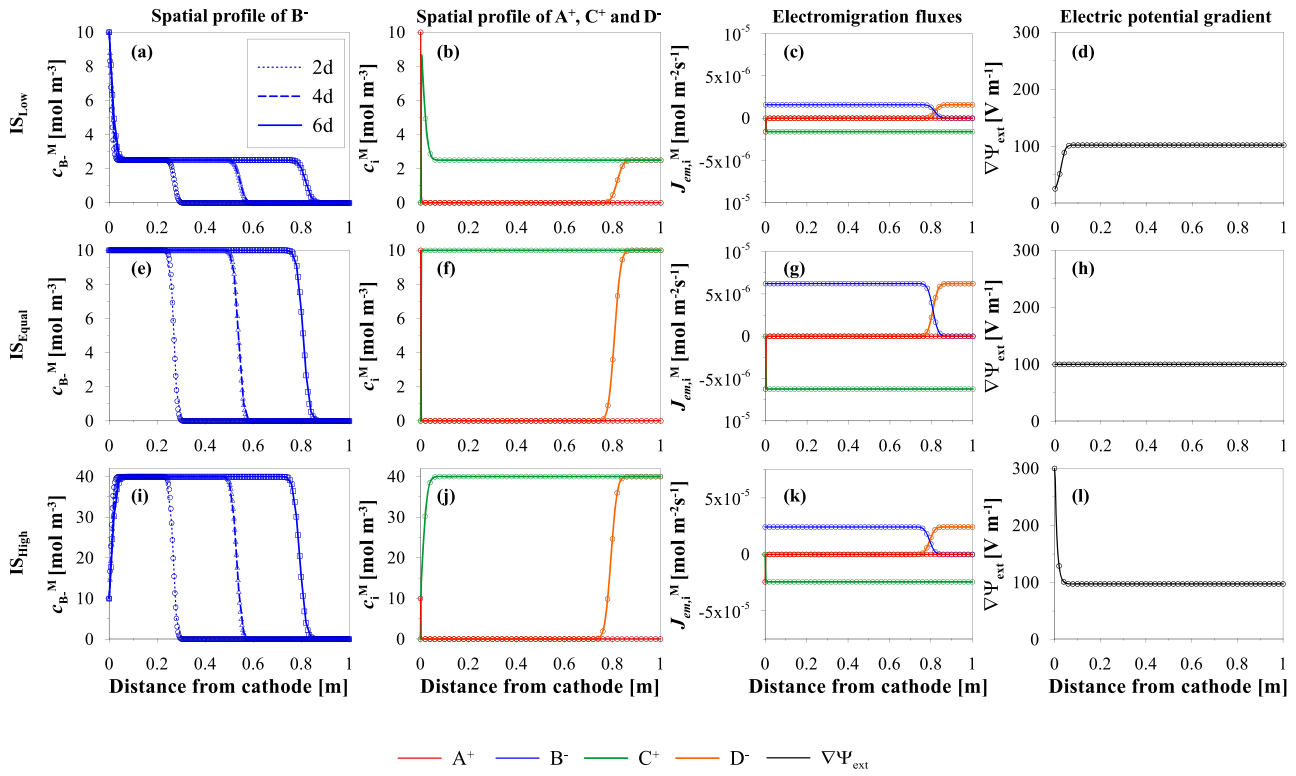

Fig. 5. Simulation exercise 4. Results of the cases IS_{Low} (1st row), IS_{Equal} (2nd row) and IS_{High} (3rd row). 1st column: Spatial distribution of B^- evaluated at 2 h, 4 h and 6 h. 2nd column: Spatial distributions of the A^+, $C^+$and D^- concentration. 3rd column: Spatial distributions of the electromigration fluxes of A^+, B^-, $C^+$and D^-. 4th column: Spatial distributions of $\nabla\psi_{ext}$. The results presented in the last three columns are evaluated at 6 h. Markers: Results of Sprocati and Rolle [17]; Lines: Proposed double-porosity M4EKR model.

reference base. The simulation indicates that the transport of B^- from the catholyte is dependent on the initial concentration of charged species in the porewater, or in other words, the ionic strength of the solution. Even though the concentration of species in the catholyte is 10^{-2} mol kg^{-1}_{water}, the concentration of the B^- anion is stabilized at values equivalent to those of the species of opposite sign contained in the porewater: 2.5×10^{-3} mol kg^{-1}_{water} in IS_{Low} and 4.0×10^{-2} mol kg^{-1}_{water} in IS_{High} scenarios, respectively. This behavior is due to the electroneutrality condition of the system and the behavior of the electrode reservoirs acting as a source/sink of species with constant concentration. Hence, the concentration profiles of the B^- and D^- anions in the soil complement each other and are compensated by the only positively charged species present in the soil, the C^+ cation. The outcomes of this test and the comparison with the previous study [15] show that the proposed M4EKR model can accurately describe EK transport in single-domain porous media.

4.3. Electrokinetic transport in double-porosity media

The last simulation exercise (SE 5) allowed us to illustrate the unique capability of the proposed M4EKR approach to simulate EK transport in double-porosity materials. Specifically, we considered the three scenarios with different ionic strength illustrated in the previous section, but now electrokinetic transport occurs in a porous medium characterized by a macro- and microstructural levels. The aim of this analysis is twofold: (i) to evaluate the behavior of the system when considering an additional modeling level where the species are influenced by the surface charge of the porous medium (microstructure) and (ii) to determine the influence of the transport of species through this additional modeling level.

4.3.1. Restricted microstructural transport

Fig. 6 presents the main results obtained under the assumption of "restricted microstructural transport".

Comparing the results evaluated at macrostructural level with those obtained in the simulation EK single-porosity media (SE 4), the only difference between the approaches can be seen in the magnitude of the macrostructural electromigration flux (Fig. 6b, f and j). Although the concentration is the same, the macrostructural electromigration flux magnitudes are smaller, namely a half of the original ones (Fig. 5c, g and k). This behavior can be explained considering that the porosity associated with the macrostructural modeling level is 0.2, half of the total porosity for the single-porosity case (SE 4). The porosity is present both in the definition of the mass per unit volume (Eq. (6)) and in the definition of all the fluxes through the expression of the effective diffusion coefficient (Eq. (13)). Therefore, since the source-sink term is equal to zero, the porosity is a factor that multiplies all terms on both sides of the mass balance equation (Eq. (5)). Halving the porosity does not affect the final outcome of the mass distribution, as long as the transport in the microstructural domain is restricted. This statement can be verified in Fig. 6d, h and l, where zero fluxes can be observed at the microstructural level. In addition, the concentration of the species at this level is very different with respect to the macrostructural level. Specifically, there is an increase in the concentration of the cation C^+ (several orders of magnitude higher than the concentration of the other species) to compensate the negative charge of the MX-80 and to equilibrate the macrostructural concentration by Donnan equilibrium. This concentration remains almost constant in time and space (Fig. 6c, g and k), and consequently does not have any effect on the macrostructural mass balance.

4.3.2. Free microstructural transport

Fig. 7 presents the main results obtained by considering "free microstructural transport" allowing ion transport in the microstructural

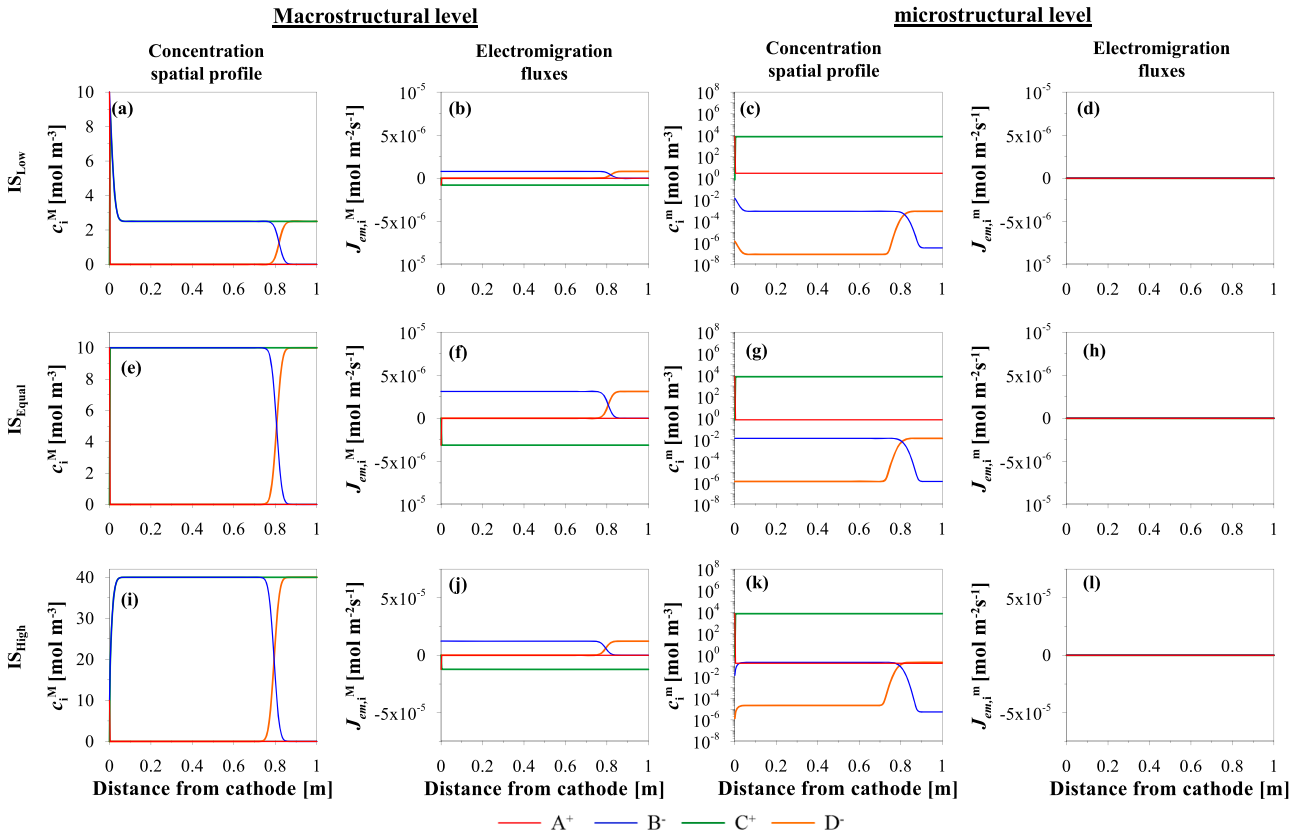

Fig. 6. Simulation exercise 5 conducted with the double-porosity M4EKR model assuming restricted microstructural transport. Simulated results of the cases IS_{Low} (1st row), IS_{Equal} (2nd row) and IS_{High} (3rd row) in Macrostructural level (Spatial distribution of: 1st column.- concentration and 2nd column.- electromigration fluxes) and microstructural level (Spatial distribution of: 3rd column.- concentration and 4th column.- electromigration fluxes) both evaluated at 6 h.

level.

In this case, significant differences are observed with respect to the single-porosity simulations in the IS_{Low} and IS_{High} scenarios. This fact indicates that transport at the microstructural level strongly influences the behavior of the EK system.

The IS_{Low} scenario assumes that initially the species concentration in the porewater of the single-porosity media or the macrostructural level of the double-porosity media is always lower than the species concentration in the catholyte. This is not fulfilled at the microstructural level where the concentration of C^+ cation is much higher and constant due to electrostatic effects associated with the surface of the double-porosity medium. This high concentration in the microstructure is responsible for the significant increase in the electromigration flux of C^+, reaching values of up to 10^{-3} mol m^{-2} s^{-1} (see Fig. 7d, h and l) notably higher than those observed both in the single-porosity system (in the order of 10^{-6} - 10^{-5} mol m^{-2} s^{-1}, SE 4, Fig. 5c, g and k) and at the macrostructural level (also in the order of 10^{-6} - 10^{-5} mol m^{-2} s^{-1}, SE 5 assuming free microstructural transport, Fig. 7b, f and j). Considering the electroneutrality condition, this high flux of positive charge generates an important charge imbalance that can only be compensated by the mobilization of the B^- anion released from the catholyte. The maximum rate at which the B^-anion can be transported, $\mathbf{j}^{L}_{em,B^-}$, is set by the maximum concentration of B^- available in this reservoir, see Eq. (10), which is orders of magnitude smaller than the one of C^+ in the domain and will therefore act as a limiting factor in the transport of species in this case. Analyzing the electromigration fluxes in the macrostructure, it is possible to observe that the maximum value achieved by $\mathbf{j}^{M}_{em,B^-}$ at the catholyte/soil interface is around 3.0×10^{-6} mol m^{-2} s^{-1}. This value directly determines the rate of transport of C^+ in this zone. On the contrary, at the porous medium/anolyte interface, the $\mathbf{j}^{M}_{em,C^+}$ is lower (around 8.0×10^{-7} mol m^{-2} s^{-1}) because in this area this value is set by the transport of the D^- anion, which is minimally influenced by the microstructural effect (same values of $\mathbf{j}^{M}_{em,D^-}$ in Figs. 6b and 7b). The domain is, therefore, divided into two zones, the one controlled by the migration of B^- (on the cathode side) and the one controlled by the migration of D^- (on the anode side), which are gradually shifted from left to right.

Similarly, the behavior observed in the IS_{High} scenario when transport within the microstructural modeling level is allowed can be explained analogously. After analyzing the spatial profiles of the B^- anion concentration (Fig. 7f) it can be seen that, again, the concentration in the area adjacent to the cathode is equal to the concentration in the catholyte, proving that this variable acts as a limiting factor when microstructural transport is not restricted. Consistently, it can be observed that in this case (where the ionic strength of the soil is higher than that of the catholyte) the opposite distribution of the electromigration fluxes is obtained. At the cathode side, $\mathbf{j}^{M}_{em,B^-}$ induces a lower flux $\mathbf{j}^{M}_{em,C^+}$ than the one at the anode side, obtaining the profiles shown in Fig. 7j.

In the IS_{Equal} scenario, no remarkable changes with respect to the single porosity simulation (SE4) are observed. The concentration of species is the same in the electrolyte reservoirs as in the soil and therefore the fluxes on the anode side and on the cathode side are consequently equal.

The behavior of the system when considering transport at the microstructural level is clearly different from that observed in single porosity media. In the latter cases, it has been found that the concentration of the porewater determines the fluxes mobilized. In the case of double-porosity media with transport in the microstructure, the limiting factor is the concentration of species in the electrolyte compartments. In

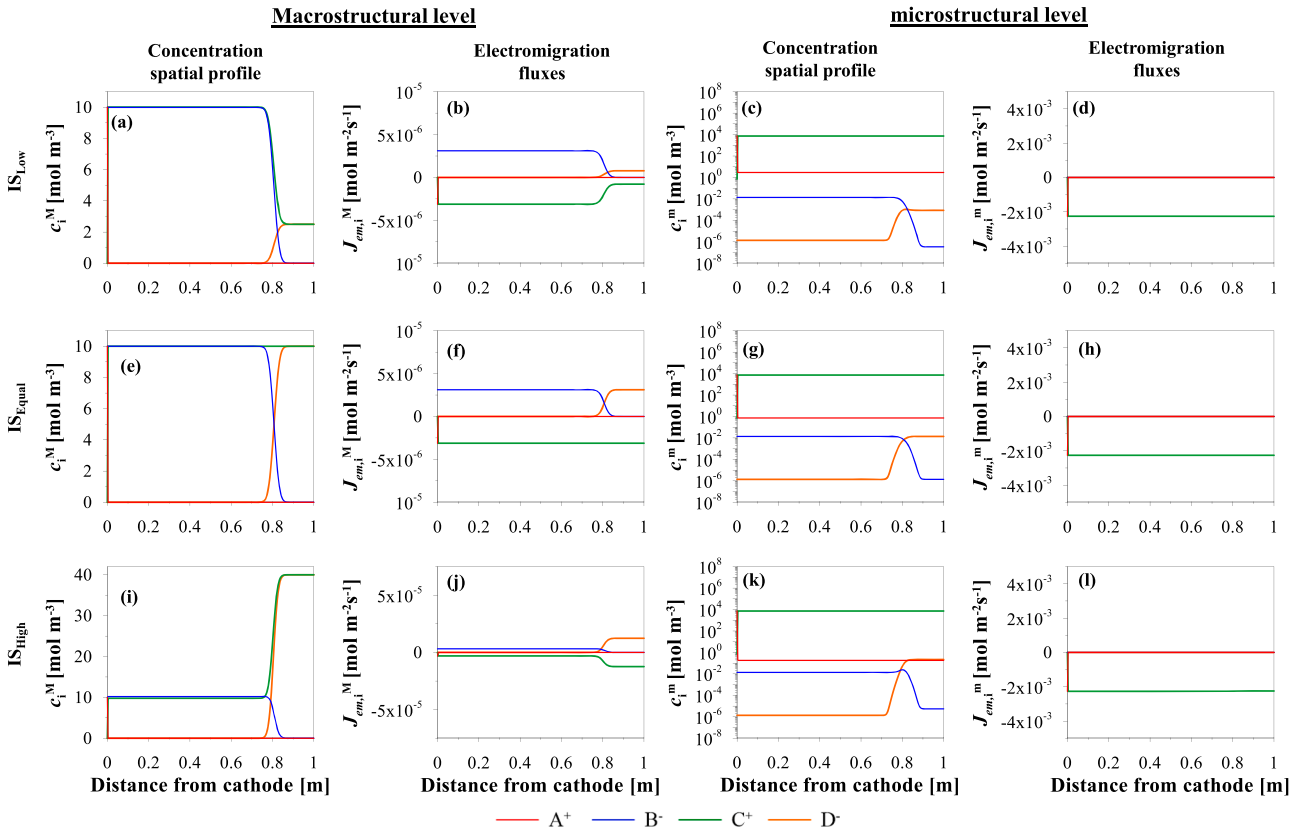

Fig. 7. Simulation exercise 5 conducted with the double-porosity M4EKR model assuming free microstructural transport. Simulated results of the cases IS_{Low} (1st row), IS_{Equal} (2nd row) and IS_{High} (3rd row) in Macrostructural level (Spatial distribution of: 1st column.- concentration and 2nd column.- electromigration fluxes) and microstructural level (Spatial distribution of: 3rd column.- concentration and 4th column.- electromigration fluxes) both evaluated at 6 h.

this case the fluxes of cations in the microstructure induce the delivery of the B^- from catholyte to the porous medium up to the maximum allowable value which is ultimately determined by the catholyte concentration.

Further variations of simulation exercise SE 5 have been carried out by varying the initial concentrations of the catholyte. For this purpose, two additional simulations have been performed employing a concentration of 15 and 30 mol m^{-3} in the catholyte. Both cases fulfill the assumptions of the Low and High scenarios: (i) for the IS_{Low} scenario both cases are higher than the 2.5 mol m^{-3} concentration of the species in the porewater and (ii) for the IS_{High} scenario both cases are lower than the 40 mol m^{-3} concentration of the species in the porewater. The main results are presented in Fig. 8.

In all cases, the concentration of C^+ in the porewater reaches the same value than the maximum available concentration of B^- in the catholyte.

5. Conclusions

In this work we illustrated the conceptualization, formulation, and implementation in the code M4EKR of an approach to model electrokinetic transport in double-porosity media. The approach is based on two modeling levels associated with the macrostructure and microstructure of the porous medium, the balance equations, the fluxes of each mass transfer process, and the electrostatic equilibrium (Donnan equilibrium) caused by the surface charge of the clay particles, have been defined. We presented different simulation exercises with single and double porosities in order to test specific features of the proposed approach. The most complex scenarios of electrokinetic transport in double-porosity media analyzed allowed us to illustrate the unique capabilities of the model and to explore the impact of micro and

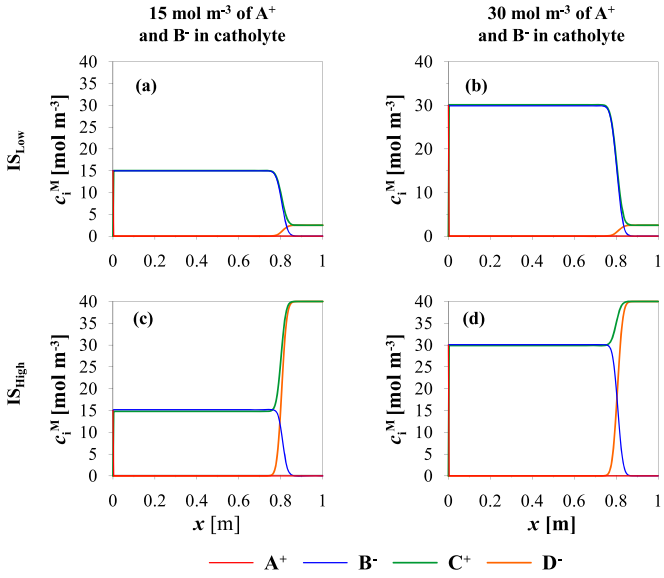

Fig. 8. Simulation exercise 5 – Additional cases with different initial concentration. Spatial distributions in macrostructural level of the concentration of A^+, B^-, C^+ and D^- species. 15 mol m^{-3} of A^+ and B^- in catholyte for (a) IS_{HLow} and (b) IS_{High}. 30 mol m^{-3} of A^+ and B^- in catholyte for (a) IS_{HLow} and (b) IS_{High}. The results presented are evaluated at 6 h.

macrostructural levels on electromigration in clay systems. The most appreciable effect of the influence of the microstructural level can be observed when the fluxes in this domain are not restricted. Greater

cation fluxes occur, resulting in a behavior clearly different from the single porosity case. This behavior could have important practical implications for the design of electrokinetic soil treatments as the composition of the electrolytes in the electrode compartments would be crucial for soil decontamination as their concentration would be the one finally applied to the porewater of the treated soil.

In real problems of electrokinetic transport in active clays the complexity is even higher. Relevant geochemical interactions are expected such as the pH buffering by carbonates [40,63] that may alter the distribution of species, Donnan equilibrium phenomena at the microstructural level [64], dissolution-precipitation of minerals [63] and a significant contribution of the liquid phase flow, either by hydraulic flow or by electroosmosis, resulting in a greater role to advective transport of chemical species [65,66]. Therefore, further modeling efforts are needed to accurately describe such complex systems and to understand and quantitatively interpret the experimental results reported by authors working in bentonites [67–69].

CRediT authorship contribution statement

Rubén López-Vizcaíno: Conceptualization, Methodology, Software, Validation, Writing – original draft, Writing – review & editing. **Virginia Cabrera:** Software, Validation, Writing – original draft. **Riccardo Sprocati:** Conceptualization, Formal analysis, Resources, Writing – review & editing. **Muhammad Muniruzzaman:** Conceptualization, Formal analysis, Resources, Writing – review & editing. **Massimo Rolle:** Conceptualization, Formal analysis, Resources, Writing – review & editing, Funding acquisition. **Vicente Navarro:** Writing – review & editing, Supervision, Project administration, Funding acquisition. **Ángel Yustres:** Conceptualization, Methodology, Software, Validation, Formal analysis, Writing – review & editing.

Declaration of Competing Interest

The authors declare that they have no known competing financial interests or personal relationships that could have appeared to influence the work reported in this paper.

Acknowledgments

The authors acknowledge funding support from (i) grant [BIA2017–89287-R] co-funded by MCIN/AEI/10.13039/501100011033 and by "ERDF A way of making Europe", (ii) grant [PID2020–118291RB-I00] funded by MCIN/AEI/10.13039/501100011033, (iii) grant [IJC-2018–035212] funded by MCIN/AEI/10.13039/501100011033, (iv) Postdoctoral grant [2022-POST-20890] co-funded by University of Castilla-La Mancha and European Social Fund plus (ESF+), (v) grant [40682] funded by Villum Fonden, and (vi) grant [1127–00013B] funded by the Independent Research Fund Denmark.

Supplementary materials

Supplementary material associated with this article can be found, in the online version, at doi:10.1016/j.electacta.2022.141139.

References

[1] Y.B. Acar, A.N. Alshawabkeh, Principles of electrokinetic remediation, Environmen. Sci. Technol. 27 (1993) 2638–2647, https://doi.org/10.1021/es00049a002.
[2] Y.B. Acar, R.J. Gale, A.N. Alshawabkeh, R.E. Marks, S. Puppala, M. Bricka, R. Parker, Electrokinetic remediation: basics and technology status, J. Hazard. Mater. 40 (1995) 117–137, https://doi.org/10.1016/0304-3894(94)00066-P.
[3] A.T. Yeung, S. Datla, Fundamental formulation of electrokinetic extraction of contaminants from soil, Can. Geotech. J. 32 (1995) 569–583, https://doi.org/10.1139/t95-060.
[4] M. Malekzadeh, J. Lovisa, N. Sivakugan, An overview of electrokinetic consolidation of soils, Geotech. Geol. Eng. 34 (2016) 759–776, https://doi.org/10.1007/s10706-016-0002-1.
[5] L.M. Ottosen, I. Rörig-Dalgaard, Desalination of a brick by application of an electric DC field, Mater. Struct. 42 (2009) 961–971, https://doi.org/10.1617/s11527-008-9435-1.
[6] J. Feijoo, L.M. Ottosen, J.S. Pozo-Antonio, Influence of the properties of granite and sandstone in the desalination process by electrokinetic technique, Electrochim. Acta 181 (2015) 280–287, https://doi.org/10.1016/j.electacta.2015.06.006.
[7] L. Chu, L. Cang, Z. Sun, X. Wang, G. Fang, J. Gao, Reagent-free electrokinetic remediation coupled with anode oxidation for the treatment of phenanthrene polluted soil, J. Hazard. Mater. (2022) 433, https://doi.org/10.1016/j.jhazmat.2022.128724.
[8] L. Chu, L. Cang, G. Fang, Z. Sun, X. Wang, D. Zhou, J. Gao, A novel electrokinetic remediation with in-situ generation of H2O2 for soil PAHs removal, J. Hazard. Mater. (2022) 428, https://doi.org/10.1016/j.jhazmat.2022.128273.
[9] K.R. Reddy, C. Cameselle, Electrochemical Remediation Technologies For Polluted Soils, Sediments and Groundwater, John Wiley and Sons, 2009, https://doi.org/10.1002/9780470523650.
[10] R. López-Vizcaíno, Á. Yustres, V. Cabrera, V. Navarro, Conceptual and mathematical modeling of the transport of pollutants in soil by Electric Fields, in: M.A. Rodrigo, E. Vieira Dos Santos (Eds.), Electrochemically Assisted Remediation of Contaminated Soils. Fundamentals, Technologies, Combined Processes and Pre-Pilot and Scale-Up Applications, Springer International Publishing, 2021, https://doi.org/10.1007/978-3-030-68140-1_4.
[11] M. Anouti, Room-temperature molten salts: protic ionic liquids and deep eutectic solvents as media for electrochemical application. Electrochemistry in Ionic Liquids: Volume 1: Fundamentals, Springer International Publishing, 2015, pp. 217–252, https://doi.org/10.1007/978-3-319-13485-7_7.
[12] R. Sprocati, M. Masi, M. Muniruzzaman, M. Rolle, Modeling electrokinetic transport and biogeochemical reactions in porous media: a multidimensional Nernst–Planck–Poisson approach with PHREEQC coupling, Adv. Water Resour. 127 (2019) 134–147, https://doi.org/10.1016/j.advwatres.2019.03.011.
[13] C.A.J. Appelo, Solute transport solved with the Nernst-Planck equation for concrete pores with 'free' water and a double layer, Cem. Concr. Res. 101 (2017) 102–113, https://doi.org/10.1016/j.cemconres.2017.08.030.
[14] C.A.J. Appelo, P. Wersin, Multicomponent diffusion modeling in clay systems with application to the diffusion of tritium, iodide, and sodium in opalinus clay, Environmen. Sci. Technol. 41 (2007) 5002–5007, https://doi.org/10.1021/es0629256.
[15] M. Muniruzzaman, M. Rolle, Modeling multicomponent ionic transport in groundwater with IPhreeqc coupling: electrostatic interactions and geochemical reactions in homogeneous and heterogeneous domains, Adv. Water Resour. 98 (2016) 1–15, https://doi.org/10.1016/j.advwatres.2016.10.013.
[16] M. Muniruzzaman, C.M. Haberer, P. Grathwohl, M. Rolle, Multicomponent ionic dispersion during transport of electrolytes in heterogeneous porous media: experiments and model-based interpretation, Geochim. Cosmochim. Acta 141 (2014) 656–669, https://doi.org/10.1016/j.gca.2014.06.020.
[17] R. Sprocati, M. Rolle, Charge interactions, reaction kinetics and dimensionality effects on electrokinetic remediation: a model-based analysis, J. Contam. Hydrol. 229 (2020), 103567, https://doi.org/10.1016/j.jconhyd.2019.103567.
[18] S. Pamukcu, Electrochemical transport and transformations, electrochemical remediation technologies for polluted soils, sediments and groundwater, John Wiley & Sons, Inc (2009) 29–64, https://doi.org/10.1002/9780470523650.ch2.
[19] J.M. Paz-García, B. Johannesson, L.M. Ottosen, A.B. Ribeiro, J.M. Rodríguez-Maroto, Modeling of electrokinetic processes by finite element integration of the Nernst-Planck-Poisson system of equations, Sep. Purif. Technol. 79 (2011) 183–192, https://doi.org/10.1016/j.seppur.2011.02.023.
[20] R. Sprocati, J. Flyvbjerg, N. Tuxen, M. Rolle, Process-based modeling of electrokinetic-enhanced bioremediation of chlorinated ethenes, J. Hazard. Mater. 397 (2020), 122787, https://doi.org/10.1016/j.jhazmat.2020.122787.
[21] C.A.J. Appelo, Chemical reactions that accompany electro-migration and electro-remediation of contaminated soils, URL: https://www.hydrochemistry.eu/exmpls/electro_dif.html (26 May 2022), (2010).
[22] C.I. Steefel, C.A.J. Appelo, B. Arora, D. Jacques, T. Kalbacher, O. Kolditz, V. Lagneau, P.C. Lichtner, K.U. Mayer, J.C.L. Meeussen, S. Molins, D. Moulton, H. Shao, J. Šimůnek, N. Spycher, S.B. Yabusaki, G.T. Yeh, Reactive transport codes for subsurface environmental simulation, Comput. Geosci. 19 (2015) 445–478, https://doi.org/10.1007/s10596-014-9443-x.
[23] M. Muniruzzaman, M. Rolle, Impact of diffuse layer processes on contaminant forward and back diffusion in heterogeneous sandy-clayey domains, J. Contam. Hydrol. (2021) 237, https://doi.org/10.1016/j.jconhyd.2020.103754.
[24] M. Muniruzzaman, M. Rolle, Multicomponent ionic transport modeling in physically and electrostatically heterogeneous porous media with phreeqcRM coupling for geochemical reactions, Water Resour. Res. 55 (2019) 11121–11143, https://doi.org/10.1029/2019WR026373.
[25] P. Alt-Epping, T. Gimmi, P. Wersin, A. Jenni, Incorporating electrical double layers into reactive-transport simulations of processes in clays by using the Nernst-Planck equation: a benchmark revisited, Appl. Geochem. 89 (2018) 1–10, https://doi.org/10.1016/j.apgeochem.2017.10.018.
[26] K. Collins, Characterisation of Expansive Soil Microfabric, National Conference Publication - Institution of Engineers, Australia, 1984, pp. 37–41.
[27] K. Collins, A. McGown, The form and function of microfabric features in a variety of natural soils, Geotechnique 24 (1974) 223–254, https://doi.org/10.1680/geot.1974.24.2.223.

[28] R. Pusch, Mineral-water interactions and their influence on the physical behavior of highly compacted Na bentonite, Can. Geotech. J. 19 (1982) 381–387, https://doi.org/10.1139/t82-041.
[29] R. Pusch, L. Moreno, Saturation and permeation of buffer clay, in: Proc. 6th Int. Workshop Key Issues in Waste Isolation Research, 2001, pp. 71–81.
[30] E. Romero, A. Gens, A. Lloret, Water permeability, water retention and microstructure of unsaturated compacted Boom clay, Eng. Geol. 54 (1999) 117–127, https://doi.org/10.1016/S0013-7952(99)00067-8.
[31] E. Romero, P.H. Simms, Microstructure investigation in unsaturated soils: a review with special attention to contribution of mercury intrusion porosimetry and environmental scanning electron microscopy, Geotech. Geol. Eng. 26 (2008) 705–727, https://doi.org/10.1007/s10706-008-9204-5.
[32] E.C. Leong, S. Tripathy, H. Rahardjo, Total suction measurement of unsaturated soils with a device using the chilled-mirror dew-point technique, Geotechnique 53 (2003) 173–182, https://doi.org/10.1680/geot.53.2.173.37271.
[33] D.L. Parkhurst, and Appelo, C.A.J., Description of input and examples for PHREEQC version 3—A computer program for speciation, batch-reaction, one-dimensional transport, and inverse geochemical calculations, in: U.S.G. Survey (Ed.) Denver, USA, 2013, pp. 497.
[34] V. Navarro, L. Asensio, T. Yustres, X. Pintado, J. Alonso, An elastoplastic model of bentonite free swelling, Eng. Geol. 181 (2014) 190–201, https://doi.org/10.1016/j.enggeo.2014.07.014.
[35] T. Gimmi, P. Alt-Epping, Simulating Donnan equilibria based on the Nernst-Planck equation, Geochim. Cosmochim. Acta 232 (2018) 1–13, https://doi.org/10.1016/j.gca.2018.04.003.
[36] C. Tournassat, C.I. Steefel, Modeling diffusion processes in the presence of a diffuse layer at charged mineral surfaces: a benchmark exercise, Comput. Geosci. 25 (2021) 1319–1336, https://doi.org/10.1007/s10596-019-09845-4.
[37] C.I. Steefel, C. Tournassat, A model for discrete fracture-clay rock interaction incorporating electrostatic effects on transport, Comput. Geosci. 25 (2021) 395–410, https://doi.org/10.1007/s10596-020-10012-3.
[38] C. Tournassat, C.A.J. Appelo, Modelling approaches for anion-exclusion in compacted Na-bentonite, Geochim. Cosmochim. Acta 75 (2011) 3698–3710, https://doi.org/10.1016/j.gca.2011.04.001.
[39] V. Navarro, L. Asensio, T. Yustres, X. Pintado, J. Alonso, Volumetric deformability and water mass exchange of bentonite aggregates, Eng. Geol. 166 (2013) 152–159, https://doi.org/10.1016/j.enggeo.2013.09.011.
[40] R. López-Vizcaíno, A. Yustres, M.J. León, C. Saez, P. Cañizares, M.A. Rodrigo, V. Navarro, Multiphysics implementation of electrokinetic remediation models for natural soils and porewaters, Electrochim. Acta 225 (2017) 93–104, https://doi.org/10.1016/j.electacta.2016.12.102.
[41] Á. Yustres, R. López-Vizcaíno, V. Cabrera, V. Navarro, For electrokinetic remediation of polluted soils, E3S Web Conf. 195 (2020) 02003, https://doi.org/10.1051/e3sconf/202019502003.
[42] T.A. Hueckel, Water-mineral interaction in hygromechanics of clays exposed to environmental loads: a mixture-theory approach, Can. Geotech. J. 29 (1992) 1071–1086, https://doi.org/10.1139/t92-124.
[43] E.E. Alonso, V. Navarro, Microstructural model for delayed deformation of clay: loading history effects, Can. Geotech. J. 42 (2005) 381–392, https://doi.org/10.1139/t04-097.
[44] Á. Yustres, R. López-Vizcaíno, V. Cabrera, M.A. Rodrigo, V. Navarro, Donnan-ion hydration model to estimate the electroosmotic permeability of clays, Electrochim. Acta 355 (2020), 136758, https://doi.org/10.1016/j.electacta.2020.136758.
[45] K. Kontturi, L. Murtomäki, J.A. Manzanares, Ionic Transport Processes. Electrochemistry and Membrane Science, OUP, Oxford, 2008.
[46] B.P. Boudreau, F.J.R. Meysman, J.J. Middelburg, Multicomponent ionic diffusion in porewaters: coulombic effects revisited, Earth Planet. Sci. Let. 222 (2004) 653–666, https://doi.org/10.1016/j.epsl.2004.02.034.
[47] M. Rolle, R. Sprocati, M. Masi, B. Jin, M. Muniruzzaman, Nernst-Planck-based description of transport, coulombic interactions, and geochemical reactions in porous media: modeling approach and benchmark experiments, Water Resour. Res. 54 (2018) 3176–3195, https://doi.org/10.1002/2017WR022344.
[48] P. Alt-Epping, C. Tournassat, P. Rasouli, C.I. Steefel, K.U. Mayer, A. Jenni, U. Mäder, S.S. Sengor, R. Fernández, Benchmark reactive transport simulations of a column experiment in compacted bentonite with multispecies diffusion and explicit treatment of electrostatic effects, Comput. Geosci. 19 (2015) 535–550, https://doi.org/10.1007/s10596-014-9451-x.
[49] C. Tournassat, C.I. Steefel, T. Gimmi, Solving the Nernst-Planck Equation in Heterogeneous Porous Media With Finite Volume Methods: averaging Approaches at Interfaces, Water Resour. Res. 56 (2020), https://doi.org/10.1029/2019wr026832.
[50] M. Masi, A. Ceccarini, R. Iannelli, Multispecies reactive transport modelling of electrokinetic remediation of harbour sediments, J. Hazard. Mater. 326 (2017) 187–196, https://doi.org/10.1016/j.jhazmat.2016.12.032.
[51] H.S. White, Ions, electrodes and membranes. By J. Koryta, John Wiley & Sons, New York, 2nd ed., 1992, AIChE J. 38 (1992), https://doi.org/10.1002/aic.690380220, 315-315.
[52] M. Mascia, S. Palmas, A.M. Polcaro, A. Vacca, A. Muntoni, Experimental study and mathematical model on remediation of Cd spiked kaolinite by electrokinetics, Electrochim. Acta 52 (2007) 3360–3365. http://doi.org/10.1016/j.electacta.2006.04.066.
[53] D.K. Cheng, Field and Wave Electromagnetics, Pearson Education Limited, 2013.
[54] J. Newman, K.E. Thomas-Alyea, Electrochemical Systems, Wiley, 2012.
[55] F. Gagnon, D. Ziegler, M. Fafard, Electrochemical modelling using electroneutrality equation as a constraint, J. Appl. Electrochem. 44 (2014) 361–381, https://doi.org/10.1007/s10800-014-0662-6.
[56] R.A. Jacobs, R.F. Probstein, Two-Dimensional Modeling of Electroremediation, AIChE J. 42 (1996) 1685–1696, https://doi.org/10.1002/aic.690420620.
[57] S. Pamucku, Electrochemical transport and transformations, Electrochemical Remediation Technologies for Polluted Soils, Sedim. Groundwater (2009).
[58] M.T. Van Genuchten, Analytical solutions of the one-dimensional convective-dispersive solute transport equation, US Department of Agriculture, Agricul. Res. Serv. (1982).
[59] O. Karnland, S. Olsson, U. Nilsson, Mineralogy and sealing properties of various bentonites and smectite-rich clay materials, SKB Technical Report, TR-06-30 (2006). https://skb.se/upload/publications/pdf/TR-06-30.pdf.
[60] L. Kiviranta, S. Kumpulainen, Quality control and characterization of bentonite materials, POSIVA - Working Report 2011-84, 2011, pp. 102.
[61] L. Kiviranta, S. Kumpulainen, X. Pintado, P. Karttunen, T. Schatz, Characterization of Bentonite and Clay Materials 2012-2015, POSIVA, 2018, p. 154.
[62] R. Sprocati, A. Gallo, R. Sethi, M. Rolle, Electrokinetic Delivery of Reactants: pore Water Chemistry Controls Transport, Mixing, and Degradation, Environmen. Sci. Technol. 55 (2021) 719–729, https://doi.org/10.1021/acs.est.0c06054.
[63] R. López-Vizcaíno, E.V. dos Santos, A. Yustres, M.A. Rodrigo, V. Navarro, C. A. Martínez-Huitle, Calcite buffer effects in electrokinetic remediation of clopyralid-polluted soils, Sep. Purif. Technol. 212 (2019) 376–387, https://doi.org/10.1016/j.seppur.2018.11.034.
[64] O. Karnland, M. Birgersson, M. Hedström, Selectivity coefficient for Ca/Na ion exchange in highly compacted bentonite, Phys. Chem. Earth 36 (2011) 1554–1558, https://doi.org/10.1016/j.pce.2011.07.023.
[65] G. De la Morena, L. Asensio, A. Yustres, V. Navarro, Educational utility of software development in engineering teaching. the example of an unsaturated soil water flow code, in: L.G. Chova, A.L. Martinez, I.C. Torres (Eds.), Inted 2017: 11th International Technology, Education and Development Conference, 2017, pp. 6606–6611.
[66] Á. Yustres, R. López-Vizcaíno, C. Sáez, P. Cañizares, M.A. Rodrigo, V. Navarro, Water transport in electrokinetic remediation of unsaturated kaolinite. Experimental and numerical study, Sep. Purif. Technol. 192 (2018) 196–204, https://doi.org/10.1016/j.seppur.2017.10.009.
[67] S. Tanaka, N. Noda, S. Sato, T. Kozaki, H. Sato, K. Hatanaka, Electrokinetic study of migration of anions, cations, and water in water-saturated compacted sodium montmorillonite, J. Nucl. Sci. Technol. 48 (2011) 454–462, https://doi.org/10.1080/18811248.2011.9711719.
[68] S. Tanaka, Gypsum precipitation enhanced by electrokinetic method and porewater chemistry in compacted montmorillonite, Appl. Clay Sci. 161 (2018) 482–493, https://doi.org/10.1016/j.clay.2018.05.011.
[69] S. Tanaka, Electrokinetic control of the growth of gypsum aggregates in compacted montmorillonite, Appl. Clay Sci. (2019) 181, https://doi.org/10.1016/j.clay.2019.105206.